EXPERIMENTAL INVESTIGATIONS OF THE INTERACTION OF SHOCK WAVES IN SOILS CONTAINING OBSTACLES

V. I. Kuznetsov and G. M. Lyakhov

Zhurnal Prikladnoi Mekhaniki i Tekhnicheskoi Fiziki, No. 2, pp. 90-96, 1966

ABSTRACT: A model of water-saturated soil as an ideal liquid has already been proposed [1]. Experimental investigations of shock waves [2] have shown that for small stresses in water-saturated soil features of a solid plastic body begin to manifest themselves. As regards its properties the soil approximates to the model proposed in [3].

The results of tests on the interaction of a plane shock wave in the soil with a moving obstacle are given below. As a development of papers [2, 4, 5] an approximate solution is given for the problem of the interaction of waves with an obstacle. At high pressures the ground is regarded as nonlinearly elastic, and at low pressures as a plastic medium. A similar approach may be applied to water-saturated and nonsaturated soils when the wave is a shock wave. Experimental values of the parameters of motion of the obstacle are compared with the results of calculation.

1. Experimental conditions. The tests were carried out under field conditions in water-saturated soil obtained by pouring quarry sand with slightly rounded grains into a pit filled with water. The water level in the pit remained constant during the whole time that the tests were carried out.

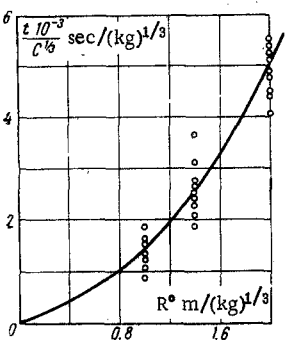

Fig. 1

The density of the soil (allowing for the water and air contained in the pores) was $\rho_0 = 1.96-2.02 \cdot 10^3$ kg/m^3. The entrapped air content α_1 comprised 0.015-0.025 of the over-all volume. The granulometric composition is given below

$\delta \geqslant 1$	1—05	0.5—0.25	0.25—0.1	0.1—0.05	0.05 [mm]
$\beta = 8-12$	10—12	25—30	30—40	4—8	2—3 [%].

Here δ is the diameter of the particles, β their percentage content.

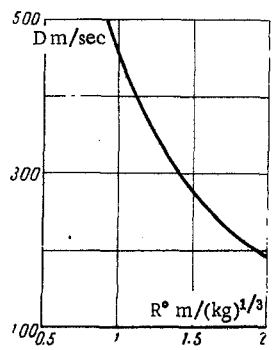

Fig. 2

The laws of plane wave propagation and interaction with obstacles in the one-dimensional formulation are determined by the law of dynamic compression of the medium. Thus the tests included measurements of wave parameters for waves formed in the soil upon explosion of a buried concentrated charge. From a knowledge of these parameters the law of dynamic compressibility of the ground was determined with the help of the well-known relationships at the front of a shock wave expressing the conservation of mass and momentum.

The interaction of waves with a moving obstacle—a concrete cube of side length $l = 1$ m—was investigated in the same soils, but with plane charges detonated on the surface of the ground over the obstacle. On explosion plane waves were formed. The loads acting on the cube and the parameters of its motion were determined in the tests.

2. Experimental determination of the compressibility of the soil and choice of a system of calculation. The maximum pressure at the front of the shock wave p, corresponding to its direction of motion, the velocity of the front D and the initial density of the medium ρ_0 are related to the deformation of the medium at the front by the familiar relation

$$\varepsilon = -\frac{p}{\rho_0 D^2}, \qquad \varepsilon = \frac{\rho_0 - \rho}{\rho} \qquad (2.1)$$

Here ρ is the current density of the medium.

In the tests where buried concentrated charges of compressed TNT were exploded the pressure p and time t of arrival of the wave front were measured at points situated at different distances R from the explosion center.

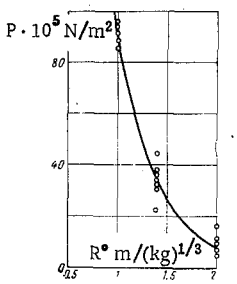

Fig. 3

The law of motion of the wave front (pressure maximum) is represented in Fig. 1. The relative distance R° is represented on the abscissa and in the conditions of spherical symmetry is equal to

$$R^\circ = RC^{-1/3} \text{ m/kg}^{1/3}.$$

Figure 2 gives a graph of the propagation velocity of the pressure maximum as a function of the relative distance, constructed in accordance with Fig. 1.

The tests showed that for $p > 5-6 \cdot 10^5$ newton/m^2 the wave has a pressure discontinuity at the front so that the velocities of wave front propagation and the pressure maximum coincide.

Figure 3 shows the results obtained in the tests for the maximum pressure at the front of the shock wave as a function of the relative distance. To the first approximation this function may be written analytically in a form satisfying the principle of similarity

$$p = 90 (R^\circ)^{-2.6}. \qquad (2.2)$$

A graph of p as a function of the deformation ε, expressing the law of dynamic compression of the soil, is given in Fig. 4 (curve 1). The graph was constructed in accordance with (2.1) from the experimental values of p and D given in Figs. 2 and 3. No curve is given for $p < 5 \cdot 10^5$ newton/m^2, since the wave is not a shock wave and equation (2.1) is inapplicable. In the pressure interval $p > 5 \cdot 10^5$ newton/m^2 an elastic wave is not formed in front of the plastic (shock)

wave in the soil under investigation.

The construction of soil compression diagrams from experimental values of shock wave parameters is considered in [2, 6], etc.

In carrying out the tests simultaneous measurements were made of the pressure acting in the direction of wave motion p and in the perpendicular direction p_τ. This allowed the magnitude of the lateral pressure coefficient k_τ to be determined for different values of the normal pressure p. The values obtained for k_τ are given below.

$p10^{-5}=$	5	10	20	30 [N/m²]
k_τ =0.75	0·88	0·95	1	$\left(k_\tau=\frac{p_\tau}{p}\right)$.

Since k_τ was known from the test, the law of compressibility of the soil could be represented in the form of the mean normal stress σ as a function of the deformation

$$\sigma = {}^1/_3(1 + 2k_\tau)p = f(\varepsilon).$$

For k_τ close to unity, the functions $p(\varepsilon)$ and $\sigma(\varepsilon)$ coincide in the first approximation.

For $p > p_n = 10 \cdot 10^5$ newton/m² the lateral pressure coefficient is practically equal to unity, i.e., the soil behaves like a liquid. As the stress decreases, the quantity k_τ also decreases, and the soil acquires the properties of a solid.

The value of the pressure p_n at which the properties of water-saturated soil change depends on its entrapped air content. The less air, the smaller is this pressure. Tests [2] show that for $\alpha = 0.001$ we have $p_n = 1\text{–}2 \cdot 10^5$ N/m².

Tests show [7] that in soils which are not water-saturated the weight distribution curves $\sigma_1(\varepsilon)$, where $\sigma_1 = -p$ differ little from the lines $\varepsilon = \text{const}$, and the residual deformations are close to the maximum. If we consider that the compression curves are such [2, 5] that $d\sigma_1/d\varepsilon > 0$, $d^2\sigma_1/d\varepsilon^2 < 0$ for small pressures, and $d\sigma_1/d\varepsilon > 0$, $d^2\sigma_1/d\varepsilon^2 > 0$ for large pressures (exceeding several atmospheres), we find that as the stress increases the intensity of residual deformation increase in soils grows at first and afterwards falls off. This is taken into account in the soil model applied below.

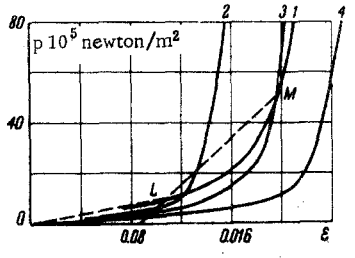

Fig. 4

Figure 4 also represents the function $p(\varepsilon)$ calculated in accordance with the equation of state of water-saturated soil as an ideal three-component liquid given in [1]:

$$p = \rho_0\left\{\alpha_1\left(\frac{p}{p_0}\right)^{-1/\gamma_1} + \alpha_2\left[\frac{\gamma_2(p-p_0)}{\rho_2 c_2^2} + 1\right]^{-1/\gamma_2} + \alpha_3\left[\frac{\gamma_3(p-p_0)}{\rho_3 c_3^2} + 1\right]^{-1/\gamma_3}\right\}^{-1}, \qquad (2.3)$$

$$\rho_0 = \alpha_1\rho_1 + \alpha_2\rho_2 + \alpha_3\rho_3 . \qquad (2.4)$$

Here α_1, α_2, α_3 are the volume content of entrapped air, water and solid component, respectively, ρ_1, ρ_2, ρ_3 are the densities of the components in the initial state; c_1, c_2, c_3 is the velocity of sound in the components in the initial state; γ_1, γ_2, γ_3 are the iso-entropy coefficients of the components taken equal to 1.4, 3, 3, ρ_0 is the density of the soil in the initial state.

Curves 2, 3, and 4 correspond to calculations for α_1, equal to 0.015, 0.020 and 0.025, i.e., for minimum, medium and maximum air content obtained in the tests.

It follows from a comparison of the curves in Fig. 4 that the experimental curve 1 of the dynamic compression for a pressure in excess of $15\text{–}20 \cdot 10^5$ N/m² corresponds to the theoretical curve 3. This shows that the compressibility of the soil under investigation is determined for $p > 15\text{–}20 \cdot 10^5$ N/m² by its compressibility as a three-component medium and is satisfactorily described by equation (2.3).

The departure of the experimental curve 1 from the theoretical 3 for small pressures is connected with the fact that in this case the compressibility of the soil is determined not only by its compressibility as a three-component medium, but also by the compressibility of the skeleton. Thus the experimental values of the deformation are less than those calculated on the basis of the three-component liquid model.

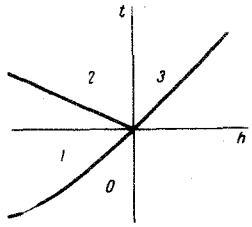

Fig. 5

In carrying out the calculations we make use of the approximate diagram $p(\varepsilon)$ (Fig. 4), corresponding to loading and unloading of the ground. We assume that loading takes place in two rectilinear sections (broken line) approximating curve 1, calculated from the values of the shock wave parameters

$$p = -A_1^2(V - V_0), \quad p \leqslant p_n \text{ first section } OL$$
$$p = -A_2^2(V - V_n) + p_n, \quad p \geqslant p_n \text{ second section } LM \qquad \left(V = \frac{1}{\rho}\right) \qquad (2.5)$$

For any values of the maximum pressure, unloading occurs along lines parallel to the straight line LM. This takes into account the irreversibility of deformations at small pressures. In accordance with test data we take

$$p_n = 10 \cdot 10^5 \text{ newton/m}^2,$$
$$A_1 = 4.25 \cdot 10^5 \text{ kg/sec} \cdot \text{m}^2,$$
$$A_2 = 9.5 \cdot 10^5 \text{ kg/sec} \cdot \text{m}^2.$$

For $p > p_n$ the residual deformations of the soil are taken to be identical, except for the dependence on maximum pressure.

3. Calculation of interaction of wave with obstacle. Let the pressure in the incident wave at the level of the obstacle (cross section $h = 0$) for $t = 0$ increase in a step from $p_0 = 0$ to p_m, and subsequently fall off according to a given law

$$p = f(t). \qquad (3.1)$$

On the side of the incident wave the properties of the medium are determined by equations (2.5), and beyond the obstacle for loading and unloading

$$p = -A^{*2}(V - V_0). \qquad (3.2)$$

We take $A^* = A_1$ in the calculations.

We employ Lagrangian coordinates (mass h and time t) and represent the region of the incident wave by the profile 1 in the h, t plane, the reflected wave by profile 2, and the wave passing beyond the obstacle by 3 (Fig. 5). The regions 1 correspond to negative values of h and t.

The flow in these regions is determined by the solution of the fundamental equations of motion

$$\frac{\partial u}{\partial t} + \frac{\partial p}{\partial h} = 0, \qquad \frac{\partial u}{\partial h} - \frac{\partial V}{\partial t} = 0, \qquad (3.3)$$

where u is the velocity of the particles.

When the function p(V) is made linear, the solution of the basic equations has the form [2]

$$p = F_1(h - A_2 t) + F_2(h + A_2 t),$$
$$A_2 u = F_1(h - A_2 t) - F_2(h + A_2 t) \qquad (3.4)$$

where the acoustic impedance A_2 corresponds to unloading of the medium.

The functions F_1 and F_2 are determined by the initial and boundary conditions.

In accordance with [2, 4, 5], we find the solution in region 1.

To start with, we will consider the case when $p_m > p_n$. The relationships at the front of the incident shock (the boundary of regions 1.0 in Fig. 5), give

$$p = \frac{\lambda h_s^{\cdot 2}}{A_2^2 - h_s^{\cdot 2}}, \qquad u = \frac{\lambda h_s^{\cdot}}{A_2^2 - h_s^{\cdot 2}},$$
$$\lambda = -p_n + A_2^2 (V_0 - V_n) = -p_n - A_2^2 \frac{\varepsilon_n}{\rho_0}, \qquad (3.5)$$

as was shown in [5].

Here ε_n is the deformation for $p = p_n$, ρ_0 is the initial density of the medium, $h_s^{\cdot}$ is the velocity of the front in h, t coordinates. We introduce the symbols

$$\varphi_1 = \frac{h_s^{\cdot}}{A_2 - h_s^{\cdot}}, \qquad \varphi_2 = \frac{h_s^{\cdot}}{A_2 + h_s^{\cdot}}.$$

At the front

$$2F_1 = \lambda\varphi_1, \qquad 2F_2 = -\lambda\varphi_2,$$

in accordance with (3.4) and (3.5).

The velocity of the incident wave front is not constant. As it changes, the function φ_2 changes little in comparison with φ_1. We shall first find the second function F_2. For the approximation which has been introduced the velocity of the front $h_s^{\cdot}$ for $p_n < p_m < p_{n+1}$ (where p_{n+1} is the maximum pressure, corresponding to the part of the approximation considered) lies in the interval

$$A_1 \leqslant h_s^{\cdot} = \rho_0 D \leqslant \left(\frac{p_{n+1}\rho_0}{\varepsilon_{n+1}}\right)^{1/2} = w.$$

Thus

$$\frac{A_1}{A_1 + A_2} \leqslant \varphi_2 \leqslant \frac{w}{A_2 + w}.$$

Hence we may take

$$\varphi_2 = \frac{1}{2}\left[\frac{A_1}{A_1 + A_2} + \frac{w}{A_2 + w}\right]$$

to the first approximation. From the condition at the cross section h = = 0 we find the first function in region 1

$$F_1(h - A_2 t) = -F_2 + f\left(\frac{-h + A_2 t}{A_2}\right). \qquad (3.6)$$

From this we have the solution in region 1

$$p = f\left(\frac{-h + A_2 t}{A_2}\right), \qquad u = \frac{1}{A_2}\left[f\left(\frac{-h + A_2 t}{A_2}\right) - 2F_2\right].$$

We shall find the equation of motion of the obstacle. The states of the medium at and ahead of the reflected wave front lie on one straight loading line, since $p_m > p_n$. Thus the velocity of the reflected wave front is equal to the acoustic impedance

$$h_s^{\cdot} = -\left(\frac{p - p_1}{V - V_0}\right)^{1/2} = -A_2.$$

Here p_1 and V_1 are the pressure and volume in the region 1. We obtain from the relationships at the reflected wave front

$$p + A_2 u = p_1 + A_2 u_1.$$

It follows from this that the function $F_1(h - A_2 t)$ passes from region 1 to region 2.

The pressure on the obstacle in region 2 is, in view of (3.4) and (3.6),

$$p = 2F_1(-A_2 t) - A_2 u = -2F_2 + 2f(t) - A_2 u,$$
$$2F_2 = -\lambda\varphi_2. \qquad (3.7)$$

Here u is the velocity of the obstacle, equal to the velocity of the particles of the medium which are in contact with it.

For t = 0 the press ure on the obstacle is $p = 2[f(t) - F_2(-A_2 t)]$.

In view of (3.2), in region 3

$$p^* = A^* u \qquad (3.8)$$

for all particles, and consequently on the obstacle too.

Hence we have the equation of motion of the obstacle

$$mu^{\cdot} = p - p^* = -2F_2 + 2f(t) - (A_2 + A^*)u \qquad (3.9)$$

where m is the mass of the obstacle per unit area.

If the pressure change in the initial cross section is given in the form

$$p = f(t) = p_m(1 - t/\theta), \qquad (3.10)$$

then the equation of motion of the obstacle is

$$u^{\cdot} + Cu + Bt + D = 0, \qquad B = \frac{2p_m}{m\theta},$$
$$C = \frac{A_2 + A^*}{m}, \qquad D = -\frac{2p_m}{m} + \frac{2F_2}{m}. \qquad (3.11)$$

Integrating this equation on condition that u = 0 for t = 0, we obtain the velocity of the obstacle

$$u(t) = -\frac{D}{C} - \frac{B}{C^2}(Ct - 1) + Me^{-Ct},$$
$$\left(M = -\frac{B}{C^2} + \frac{D}{C}\right). \qquad (3.12)$$

Taking into account that x = 0 for t = 0 we find for the displacement of the obstacle

$$x = \int_0^t u\,dt = \frac{M}{C}(1 - e^{-Ct}) - Mt - \frac{Bt^2}{2C}. \qquad (3.13)$$

The pressures at the front and rear boundaries of the obstacle are determined by equations (3.7) and (3.8), since the velocity of the obstacle is known. The acceleration of the obstacle is

$$u^{\cdot} = -B/C - MCe^{-Ct}. \qquad (3.14)$$

The velocity of the obstacle increases at first and then decreases. It reaches a maximum for

$$t^* = \frac{\lg(B - DC) - \lg B}{C \lg e}. \qquad (3.15)$$

We shall consider the second case when the maximum pressure at the initial cross section p_m is less than p_n, but becomes greater than p_n on reflection from the obstacle.

If the pressure is given by equation (3.10) at the cross section h = 0 then, as has been shown in [4], we obtain the solution in region 1 in the form

$$p = p_m\left(1 + \frac{A_1^2 + A_2^2}{2A_1A_2^2}\frac{h}{\theta} - \frac{t}{\theta}\right),$$
$$A_2 u = p_m\left(\frac{A_2}{A_1} + \frac{h}{A_2\theta} - \frac{A_1^2 + A_2^2}{2A_1A_2}\frac{t}{\theta}\right). \qquad (3.16)$$

The velocity of the incident wave front $h_s^{\cdot}$ is equal to A_1, and that of the reflected wave is close to A_2. Assuming that $h_s = A_2$ for the reflected wave we find from the relationships at the front that the function

$$F_1(h - A_2 t) = \frac{A_1 + A_2}{2A_1}\left[1 + \frac{A_1 + A_2}{2A_2^2\theta}(h - A_2 t)\right]p_m \qquad (3.17)$$

passes from region 1 to region 2.

From this we obtain the equation of motion of the obstacle in the form (3.11). Here

$$B = \frac{(A_1 + A_2)^2 p_m}{2A_1A_2m\theta}, \quad C = \frac{A_2 + A^*}{m}, \quad D = -\frac{A_1 + A_2}{mA_1}p_m. \qquad (3.18)$$

The velocity, displacement and acceleration of the obstacle are determined by expressions (3.12), (3.13) and (3.14) for the corresponding values of B, C, D. The pressure acting from above on the obstacle is determined by the expression

$$p = 2F_1(-A_2 t) - A_2 u.$$

The pressure from below is found in accordance with (3.8).

4. Comparison of the results of tests and calculations. The tests were carried out with flat charges laid on the surface of the ground. The dimensions of the charge were 4.5 × 4.5 m². The obstacle, a concrete cube, was set in the ground in the center of the area under the charge. The fact that the area of the charge was in excess of that

of the obstacle ensured that a plane shock wave fell on all points of the obstacle, undistorted by the influence of a rarefaction wave from layers of soil over which there was no charge.

The tests were carried out at two values of the density (thickness) of the plane charge, for which the maximum pressure in the wave incident on the obstacle was $5.5 \cdot 10^5$ and $20 \cdot 10^5$ newton/m^2.

The pressure was measured by strain-gauge sensing elements, and the velocity of the obstacle by induction velocity gauges.

In Figs. 6 and 7 the broken lines correspond to the mean experimental values, and the full lines to the values calculated from equations (3.10), (3.7), (3.8), (3.12). Figure 6 corresponds to $p_m = 5.5 \cdot 10^5$ newton/m^2, Fig. 7, to the value $p_m = 20 \cdot 10^5$ newton/m^2. Here 1 is the pressure in the incident wave at the level of the top of the obstacle, 2 is the pressure acting on the obstacle from above, 3 is the pressure acting on the obstacle from below, and 4 is the velocity of the obstacle. In the tests the greatest departures of the results of individual measurements from the mean values did not exceed 30–40%.

It is clear from the graphs that at the moment when the shock front arrives at the obstacle the pressure acting upon it from above increases in a step, and subsequently decreases. At the same moment the accelerated motion of the obstacle commences, leading to the formation of a continuous compression wave beyond it. The pressure acting on the obstacle from below is caused by its displacement and gradually increases as the velocity of the obstacle increases.

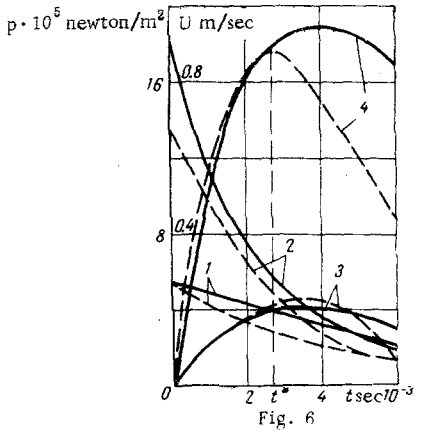

Fig. 6

For $t = t^*$ the pressure from below reaches a maximum and becomes greater than the pressure from above. Here the acceleration of the obstacle decreases to zero. For $t > t^*$ the velocity of the obstacle decreases, the pressure from above is less than from below, and the acceleration is negative. Only the experimental value of t^* is denoted in Figs. 6 and 7.

The loads experienced by the obstacle for $t > t^*$ are practically equal to the stress in the incident wave. We may assume that the obstacle is set in motion together with the ground. Comparison of the experimental and calculated values of the pressure acting from above and below on the obstacle, the values of t^*, and the velocity of the obstacle attest to the satisfactory agreement of the data of the test and calculations as regards both over-all nature and numerical values.

The curve of the dynamic compressibility of the soil was determined in this way. It has been shown that this curve corresponds to the equation of state of water-saturated ground regarded as an ideal three-component liquid for pressures in excess of $15–20 \cdot 10^5$ newton/m^2.

The loads on the obstacle obtained by calculation turned out to be in satisfactory agreement with the results of their direct measurement in the tests.

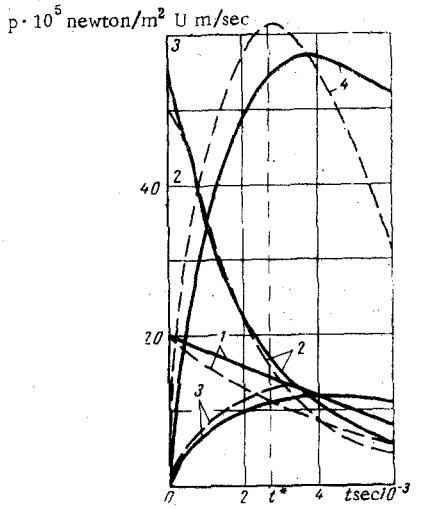

Fig. 7

We note that the international system of units has been used here. For convenience in comparing with the technical system, the pressure is given in 10^5 newton/m^2, which is equal to kg/cm^2 to the first approximation.

The authors are grateful to S. D. Mizyakin for participating in the tests.

REFERENCES

1. G. M. Lyakhov, "Shock waves in multi-component media," Izv. AN SSSR. OTN, Mekhanika i mashinostroenie, no. 1, 1959.

2. G. M. Lyakhov, Basis of Explosion Dynamics in Soils and Liquid Media [in Russian], Izd. "Nedra," 1964.

3. S. S. Grigoryan, "Basic concepts of soil dynamics," PPM, vol. 24, no. 6, 1960.

4. G. M. Lyakhov and N. I. Polyakova, "The interaction of a shock wave in an elastoplastic medium with a moving obstacle," PMTF, no. 5, 1962.

5. G. M. Lyakhov and G. I. Pokrovskii, Blast Waves in Soils [in Russian], Gosgortekhizdat, 1962.

6. S. S. Grigoryan, G. M. Lyakhov, V. V. Mel'nikov, and G. V. Rykov, "Blast waves in loess-type soil," PMTF, no. 4, 1963.

7. Z. V. Narozhnaya, "The experimental determination of the load distribution rate in soils for dynamic processes," Nauchno-tekhnicheskie problemy goreniya i vzryva, no. 1, 1965.

16 August 1965 Moscow